Molecular genetic and mitochondrial metabolic analyses confirm the suspected mitochondrial etiology in a pediatric patient with an atypical form of alternating hemiplegia of childhood

Andrea Gropman[a], Martine Uittenbogaard[b], Christine A. Brantner[c], Yue Wang[d], Lee-Jun Wong[d], Anne Chiaramello[b],*

[a] Children's National Medical Center, Division of Neurogenetics and Developmental Pediatrics, Washington, DC 20010, USA
[b] Department of Anatomy and Regenerative Biology, George Washington University School of Medicine and Health Sciences, Washington, DC 20037, USA
[c] GW Nanofabrication and Imaging Center, Office of the Vice-President for Research, George Washington University, Washington, DC 20052, USA
[d] Department of Molecular and Human Genetics, Baylor College of Medicine, Houston, TX 77030, USA

ARTICLE INFO

ABSTRACT

Alternative hemiplegia of childhood (AHC) is a rare neurodevelopmental disorder with an extensive phenotypic variability, resulting in a challenging clinical diagnosis. About 75% of AHC cases are caused by pathogenic variants mapping in the *ATP1A3*, *ATP1A2* or *GLUT1* gene, leaving many AHC patients clinically and genetically undiagnosed. In this study, we report the case of a 9-year old proband clinically diagnosed with an atypical form of AHC presenting a suspected mitochondrial etiology and an obscure genetic diagnosis. Long-range PCR followed by next generation sequencing of the proband's mitochondrial genome identified a novel mitochondrial variant, m.12302C > A, mapping in the *MT-TL2* gene with a low heteroplasmic level in blood and fibroblasts. Whole exome sequencing revealed three known and novel pathogenic variants with different parental inheritance, all involved in the mitochondrial energy metabolism and thus far not associated with AHC. Live-cell mitochondrial metabolic study showed dysregulated mitochondrial oxidative phosphorylation pathway and metabolic plasticity preventing an efficient switch to glycolysis to sustain ATP homeostasis, congruent with the suspected mitochondrial etiology. In conclusion, our comprehensive genetic and metabolic analyses suggest an oligogenic inheritance among the nuclear and mitochondrial variants for the mitochondrial etiology of proband's atypical form of AHC, thereby providing critical insight in terms of genetic clues and bioenergetic deficit. This approach also improves the diagnostic process of atypical form of AHC with an unclear genotype-phenotype correlation to personalize therapeutic interventions.

1. Introduction

The rare neurodevelopmental disorder, alternating hemiplegia of childhood (AHC) (OMIM 614820), originally described by Verret and Steele in 1971 [1], is characterized by an extensive phenotypic variability. Thus, its clinical diagnosis is challenging, but facilitated by the Aicardi criteria [2]: 1) onset before the age of 18 months; 2) recurrent transient attacks of hemiplegia involving either side; 3) paroxysmal involuntary movements, such as nystagmus, tonic attacks, dystonic posturing, choreoathetosis, and autonomic abnormalities; 4) progressive neurological deficits, such as speech disorder, behavioral deficits, cognitive impairment, and developmental delay. Our understanding of the pathophysiological mechanisms of AHC remains limited, thereby hindering the development of effective therapeutic options.

The advent of next-generation sequencing led to the discovery of the first pathogenic clue of AHC, revealing that AHC is a predominantly sporadic disorder [3]. About 75% of AHC patients harbor a *de novo* heterozygous mutation in the *ATP1A3* gene encoding the alpha 3 subunit of the neuronal Na$^+$/K$^+$ ATPase protein involved in the regulation of neuronal excitability [4–6]. Mutations in the *ATP1A2* gene encoding for the alpha 2 subunit of the Na$^+$/K$^+$ ATPase protein also cause a very small number of AHC cases (OMIM 104290) [7–9]. Thus, additional causative genes remain to be identified, resulting in patients clinically diagnosed with AHC of unknown etiology and molecular genetic diagnosis. Several studies have evoked a mitochondrial etiology in a few

---

patients with AHC. Mitochondrial abnormalities have been observed by ^{31}P magnetic resonance spectroscopy in skeletal muscle [10], while abnormal enzyme activities of the mitochondrial oxidative phosphorylation (OXPHOS) pathway were detected in skin biopsies from a handful of AHC patients [11,12].

In this study, we report the case of a 9-year-old male proband clinically diagnosed with an atypical form of AHC characterized by a suspected mitochondrial etiology and an undefined genotype-phenotype correlation. Deep sequencing of the proband's mitochondrial genome revealed a novel mitochondrial variant m.12302C > A mapping in the *MT-TL2* gene coding the mt-tRNALeu[(CUN)], while whole exome sequencing (WES) identified three pathogenic variants linked to the mitochondrial energy metabolism, but not previously associated with AHC. Live-cell mitochondrial metabolic studies showed dysregulated mitochondrial oxidative phosphorylation (OXPHOS) and metabolic flexibility, congruent with the proband's suspected mitochondrial etiology.

2. Materials and methods

2.1. Subjects

This study was approved by the Institutional Review Board of the George Washington University and Children's National Medical Center and was conducted in accordance with the ethical principles of the Declaration of Helsinki of 1975 (revised 1983). Patient skin biopsy was performed after receiving written informed consent for participation in the study and publication of the study from the legally authorized representatives (parents of the proband) included in the study.

2.2. Skin biopsy and fibroblast culture

A 3 mm skin biopsy was performed on a 9-year-old male proband, from which dermal fibroblasts were derived in Dulbecco's Modified Eagle Medium (DMEM; Gibco) supplemented with 2 mM glutamine, 2.5 mM pyruvate, 0.2 mM uridine, FGF-2 (10 ng/ml) and 20% fetal bovine serum, as described [13]. Derived dermal fibroblasts were frozen at passage 2 and never used beyond passage 10. Human primary dermal fibroblasts from a healthy subject (Cat# GM03377E) were obtained from the Coriell Cell Repositories (Camden).

2.3. Genetic testing

Total genomic DNA was isolated from blood samples from the proband and his parents to perform WES by the Medical Genetics Laboratories at Baylor, College of Medicine. The mitochondrial genome from the proband's blood and dermal fibroblasts derived from a skin biopsy performed on the proband was sequenced using long-range PCR followed by massively parallel sequencing (LR-PCR-NGS) by the Medical Genetics Laboratories at Baylor, College of Medicine, as described [14]. Genomic DNA was fragmented to be 350 base pair-long by sonication, which were ligated to the Illumina multiplex PE adapters. The adapter-ligated DNA was amplified by PCR using primers with sequencing barcodes. and library was constructed with Agilent Exome capture system (Agilent Technologies; Santa Clara, CA) following the manufacturer's instructions. Sequencing was performed using an Illumina HiSeq platform (Illumina: San Diego, CA) by synthesis chemistry with paired end read length of 100 bp. As a quality control measure, the total DNA from the proband and his parents were also analyzed by a SNP-array (Illumina HumanExome-12v1 array). The SNP data were compared with the WES data to ensure correct sample identification and to assess sequencing quality. The output data from Illumin HiSeq were converted to FastQ file by Illumina CASAVA 1.8 software and mapped by the Burrows-Wheeler Aligner program. The variant calls were performed using ATLAS-SNP and Atlas-indel developed by the Human Genome Sequencing Center (HGSC) of Baylor College of Medicine. The variant annotations were performed using the HGSC-SNP-anno and HGSC-indel-anno. The pathogenicity of variants was evaluated using the American College of Medical Genetics and Genomics (ACMGG) guidelines by board certified molecular geneticists. Computational analysis of nuclear variant's pathogenicity was performed using PolyPhen-2 and SIFT.

For the chromosomal microarray analysis, we used a combination of high resolution chromosomal microarray (CMA-HR) and CMA-SNP, which contains 60,000 SNP probes to detect copy number neutral regions of absence of heterozygosity. CMA-HR utilizes array-based comparative genomic hybridization with about 180,000 oligonucleotides covering the whole genome at the average resolution of 30 Kb, 4200 genes with all exons covered, 700 microRNAs and the entire mitochondrial genome. Quantitative imaging methods combined with analytical software were used to identify each targeted-DNA sequence as loss of copy number, gain of copy number or normal copy number.

2.4. Live-cell measurements of mitochondrial respiratory and glycolytic activity

The bioenergetic status of dermal fibroblasts derived from the patient was measured using the Seahorse Extracellular Flux XFp Analyzer (Agilent Technologies; Santa Clara, CA), as described [13]. Optimal cell density (5000/well) and the uncoupler FCCP (fluoro 3-carbonyl cyanide-methoxyphenyl hydrazine; 2 μM) were determined using the Cell Energy Phenotype Test kit. Dermal fibroblasts were seeded in triplicate on poly-D lysine-coated plates and incubated for 24 h at 37 °C in 5% CO2 atmosphere. Prior to the assay, the supplemented DMEM medium was changed to unbuffered Base Medium supplemented with 2 mM glutamine (Invitrogen), 2 mM pyruvate (Sigma; St Louis, MO), and 7.1 mM glucose (Sigma) and adjusted to pH 7.4 with NaOH. Using the XFp Mito Stress Test kit, oxygen consumption rate (OCR) and extracellular acidification rate (ECAR) were measured under basal conditions and after sequential injections of oligomycin (1 μM), FCCP (2 μM) and a mix of rotenone and antimycin A (1 μM) following the manufacturer's recommendations.

Using the Seahorse XFp real-time ATP Rate assay, we simultaneously quantified the rate of ATP produced by the two main bioenergetic pathways, OXPHOS and glycolysis, to calculate the total rate of cellular ATP production according to the manufacturer's recommendations. Prior to the assay, the culture medium is switched to the phenol-red and bicarbonate-free medium assay that contains 5 mM HEPES, 2cmM glutamine (Invitrogen), 2 mM pyruvate (Sigma), and 7.1 mM glucose (Sigma), and adjusted to pH 7.4 with NaOH. OCR and ECAR were measured under basal conditions and after sequential injections of oligomycin (1.5 μM) and a mix of rotenone and antimycin A (0.5 μM).

Using the XFp Glycolytic Rate Assay, we analyzed the glycolytic rate by quantifying the total proton efflux and the glycolytic proton efflux. Prior to the assay, the supplemented DMEM medium was changed to the XF base medium without phenol red supplemented with 2 mM glutamine, 10 mM glucose, 1 mM pyruvate, and 5.0 mM HEPES. OCR and ECAR were measured under basal conditions and after sequential injections of rotenone/antimycin A (0.5 μM) and 2-DG (50 mM).

All the data from three independent experiments, each including three technical replicates, were normalized to cell numbers after the assay and plotted as OCR (pmol/min/cell ± S.E.M.) and ECAR (mpH/min/cell ± S.E.M.) as a function of time using the Seahorse MultiReport Generator software. Statistical analyses were performed using the unpaired student *t*-test with *p*-value of less than 0.05 considered statistically significant.

2.5. Transmission electron microscopy

Fibroblasts from the proband and a healthy subject were fixed in 2.5% glutaraldehyde (Electron Microscopy Sciences), 1%
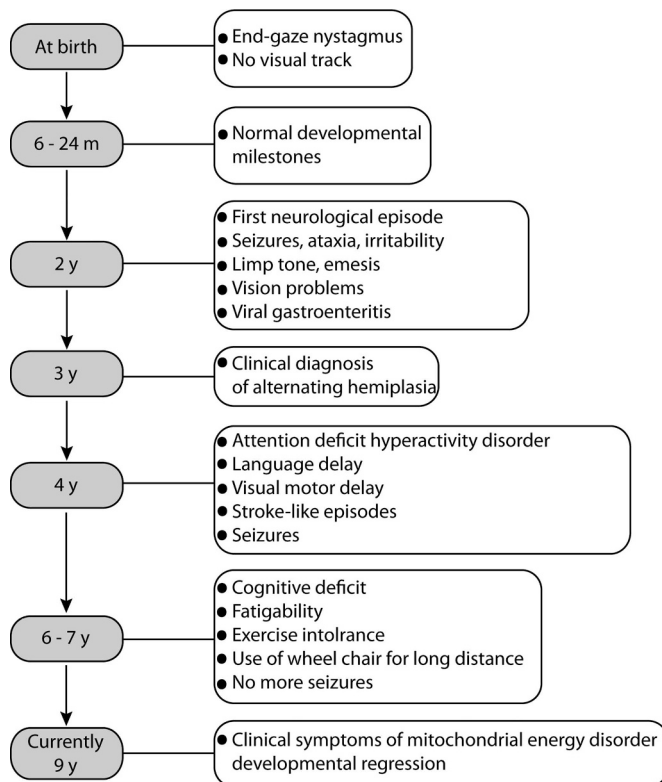
Fig. 1. Highlights of the proband's clinical history. Abbreviations: m: month; y: year.

paraformaldehyde in 0.12 M sodium cacodylate buffer (Electron Microscopy Sciences) for 20 min at room temperature followed by 40 min on ice, as described [15]. Samples were imaged with a FEI Talos F200X-transmission electron microscope (Thermo Fisher).

3. Results

3.1. Clinical history

The proband, a 9-year-old boy, has a complex history of an atypical AHC with an unclear etiology and molecular genetic diagnosis (Fig. 1). His father is Norwegian, while his mother is of Belgian, Irish, Polish and German descent. His parents are nonconsanguineous with no familial history of AHC. The proband was born in Europe at 37 weeks' gestation to a 35-year-old woman by C-section due to maternal aneurysm of unspecified nature. He weighed 2.8 kg and measured 50 cm. He had full body jaundice, reflux and colic until 4.5 months. Almost from birth, the proband exhibited end-gaze nystagmus with no visual tracking until 6 months of age. However, the proband achieved normal developmental milestones from ages 6 to 24 months.

At age of 2, the proband had his first neurological episode for about six consecutive days following a flight from Europe to the USA, which also coincided with viral gastroenteritis. He became ataxic and irritable with a limp tone and then had emesis for several hours on each of these six days while in Europe. Each neurological episode began by the proband squeezing his eyes shut, as he was having trouble with his vision. The proband underwent a brain magnetic resonance imaging (MRI), magnetic resonance spectroscopy (MRS) electroencephalogram and a lumbar puncture, which came back normal. While in preschool in Europe, the proband was found unconscious by another child in a snowdrift. He initially had a facial seizure with eye fluttering and repetitive opening and closing of the mouth, followed by a 20 min-long generalized tonic-clonic seizure. Paramedics found him unresponsive with dilated pupils for another 40 min before regaining consciousness.

For the next two days, he had difficulty communicating with his parents. An EEG, performed 24 h after the event, was normal.

Following a flight from Europe to the U.S.A., the proband had a second seizure, which was medically stopped after five minutes. While evaluated at the Epilepsy Clinic, he subsequently had a 2-day EEG, which revealed occasional intermittent brief burst of generalized spike and wave activity for which he was treated with levetiracetam and flew to Washington, D.C., his final destination. Four days after his flight, he had a stroke-like attack with right hemiparesis, characterized by limping and dragging of the right extremities for seven hours. While hospitalized at Children's National Medical Center, his EEG paradoxically showed right hemispheric (ipsilateral) slowing. He received a course of oxcarbazepine and was discharged. Following worsening episodes, the proband was hospitalized with absence episodes characterized by cessation of activity with eye fluttering, which were temporary lessened by increased dosage of oxcarbazepine. His EEG showed quite active intermittent generalized spike and wave activity associated with absence episodes that were activated by sleep. After a single dose of topiramate (82 mg), he appeared unresponsive with irritability, posturing, nystagmus and ultimately fixed and dilated pupils. EEG monitoring ruled out status epilepticus, leaving the nature of his symptoms unclear. During his second hospitalization, the proband received courses of lorazepam, fosphenytoin, phenobarbital, high dose of methylprednisolone and ultimately valproic acid (38 mg/kg/day), the latter being the most helpful. However, the proband had an acute episode of pancreatitis, presumably related to valproic acid, based on normal abdominal ultrasound with no evidence of pseudocyst or pancreatic calcifications. Finally, the proband has had intestinal problems characterized by chronic constipation and bloody diarrhea once a year.

At age of 3, the proband was making developmental progress despite his puzzling neurological disorder of alternating hemiplegia with an unclear etiology and molecular genetics. A mutation analysis for AHC failed to reveal any known pathological mutations in the coding regions of the *ATP1A3* gene, found in about 75% of AHC patients. The proband also underwent genetic testing for a comprehensive seizure panel, which showed no pathological mutations. Due to pancreatitis possibly due to valproic acid and allergy to oxcarbazepine, the proband was switched to clobazam. A few weeks later, the proband had two stroke-like episodes affecting his left side. He still had decreased balance and coordination as well as difficulties with sensory integration. His plasma and CSF lactate levels were normal.

At age of 4, the proband exhibited many signs and symptoms consistent with attention deficit hyperactivity disorder (ADHD), which further complicated his clinical history of alternating hemiplegia, a receptive and expressive language delay, visual motor delay, and minor neuromotor dysfunction. While on clobazam, he had four to six small myoclonic jerks with a tonic episode as well as two stroke-like episodes affecting his left arm, each lasting 10 min without loss of consciousness.

After turning 6, his seizures stopped and his episodes of alternating hemiplegia improved. Neurological exams showed normal strength, tone and cranial nerves. Cognitively, he had decreased attention span and limited ability to follow instructions. At the age 7, the proband showed easy fatigability to the point that the use of a wheel chair was recommended for long distances in order to preserve his energy levels for necessary activities and short-term exercises. Such exercise intolerance suggests a mitochondrial etiology. Thus, the proband underwent a cardiac evaluation, which failed to reveal any evidence of cardiomyopathy and arrhythmias.

At the age of 9, the proband still exhibits a very complex clinical history with an unclear etiology, molecular genetic diagnosis. For the last two years, he has not had a seizure-like episode while on clobazam. He now displays clinical symptoms suggestive of a mitochondrial energy disorder, including exercise intolerance, easy fatigability and developmental regression. His brain MRI remains normal (Fig. 2).
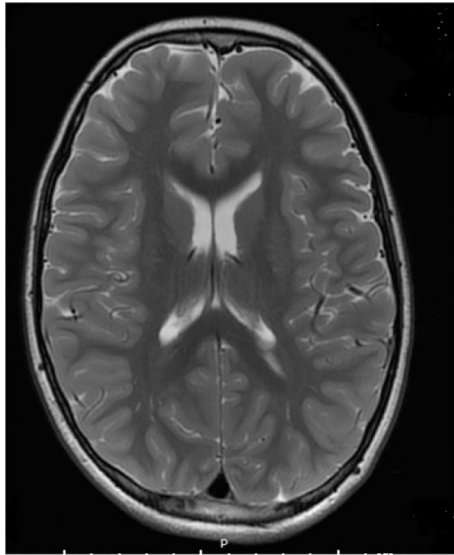
Fig. 2. Brain magnetic resonance imaging of the proband at the age of 9. The panel illustrates the T2-weighted image at the level of the basal ganglia and thalamus, showing a lack of lesions. The posterior position (p) is indicated.

3.2. Genetic diagnosis

Since his epilepsy panel and AHC mutation analysis came back negative, WES and CMA were performed using blood samples. CMA was normal and did not reveal any copy number changes associated with known microdeletion or microduplication syndromes (data not shown). The proband's mitochondrial genome sequencing by LR-PCR-NGS using the proband's blood and dermal fibroblasts did not uncover large structural rearrangements, large deletions or deleterious mitochondrial variants. We detected the rare homoplasmic variant, m.13933A > G, maping in the *ND5* gene was reported in Mitomap (www.mitomap.org) as a polymorphism with a frequency of 2700:4 (Table 1). However, our analysis revealed a novel mitochondrial variant of uncertain significance, m.12302C > A, mapping in the *MT-TL2* gene that encodes the mt-tRNALeu(CUN) (Table 1). This nucleotide change is located in the anti-codon loop of the mt-tRNALeu(CUN) immediately adjacent to the anticodon triplet. Its low heteroplasmic level was detected in blood

(2.67%) and dermal fibroblast (2.7%) derived from a skin biopsy performed on the proband (Table 1).

WES revealed three variants mapping in the galactose-1 phosphate uridylyltransferase (*GALT*) gene consistent with Duarte Galactosemia (Table 2). The lack of elevated galactose-1-phosphate levels and normal levels of GALT (4.7 nmol/h/mg) in the proband was consistent with Duarte Galactosemia, which is not related to the proband's clinical presentation of AHC. The pathogenic variant p.Q188R (rs 75,391,579) was inherited from the father, while the pathogenic variants c.-119_-166delGTCA (rs 111,033,640) and p.N314D (rs 2,070,074) were inherited from the mother (Table 2). In addition, the proband harbored the pathogenic variant, p.G2434R (rs121918593), inherited from the mother, which maps in the ryanodine receptor protein (*RYR1*) gene, known to be linked to malignant hyperthermia susceptibility (OMIM 145600) (Table 2) [16].

WES revealed three variants involved in the mitochondrial ATP metabolism, substantiating the proband's clinical symptoms suggestive of a mitochondrial etiology (Fig. 1; Table 2). The novel paternally inherited variant p.L18F (c.52C > T), which was confirmed by Sanger sequencing, maps in the *PNKD* gene encoding the myofibrillogenesis regulator 1 (MR-1) protein with a mitochondrial localization. The mutated amino acid leucine at position 18 is conserved among various species (Fig. 3A) and maps in the N-terminal 39 amino acid-long mitochondrial targeting sequence necessary for mitochondrial localization of the MR-1 protein [17]. Our computational analysis using PolyPhen-2 predicted the p.L18F variant to be probably damaging with a score of 0.999. The maternally inherited missense variant p.T207M (rs139334277) maps in the *MTO1* gene encoding the mitochondrial tRNA translation optimization 1, known to cause combined oxidative phosphorylation deficiency 10 (COXPD10; OMIM 614702). The novel paternally inherited variant, p.P63L (c.188C > T), maps in the *NDUFA2* gene encoding the NADH ubiquinone oxidoreductase subunit A2, one of the accessory subunits of the OXPHOS complex I, known to cause mitochondrial complex I deficiency nuclear type 13 manifesting as Leigh syndrome (OMIM 618235) [18] [Hoefs et al. 2008]. The mutated amino acid proline, which maps at the end of a beta strand, is conserved among various species (Fig. 3B). PolyPhen-2 predicted the p.P63L variant to be probably damaging with a score of 0.999.

Table 1

Comprehensive mtDNA analysis by massively parallel sequencing using blood sample from the proband.

Nucleotide	Gene	Base Change	Base Percentage	Codon	Amino Acid Change	Mitomap	Comments
207	OH	G > A	G:0.3 > A:99.3			reported	mtDB, 1752:123
263	HV2	A > G	A:0.2 > G:99.0			reported	mtDB, 6:1861
303	OH, CSB2	insC/CC/CCC	insC/CC/CCC:99.0			reported	303_309insC/insCC/insCCC
311	OH, CSB2	insC	insC:99.0			reported	311_315insC
750	MTRNR1 (12S)	A > G	A:0.3 > G99.5			reported	mtDB, 22:2682
1438	MTRNR1 (12S)	A > G	A:0.1 > G99.6			reported	mtDB,84:2620
2706	MTRNR2 (16S)	A > G	A:0.1 > G99.7			reported	mtDB, 525:2178
4769	ND2	A > G	A:0.2 > G:99.6	ATA > ATG	M100M	reported	mtDB, 30:2674
7028	COI	C > T	C:0.3 > T:99.5	GCC > GCT	A375A	reported	mtDB,505:2199
7930	COII	A > G	A:0.3 > G:99.5	GGA > GGG	G115G	reported	mtDB, 2701:2
8014	COII	A > T	A:0.2 > T:99.4	GTA > GTT	V143G	reported	mtDB, 2696:4
8020	COII	G > A	G:0.4 > A:98.3	CCG > CCA	P145P	reported	mtDB, 2609:95
8860	ATP6	A > G	A:0.2 > G:99.6	ACA > GCA	T112A	reported	mtDB, 6:2698
12,302	tRNALeu(CUN)	C > A	C:97.2 > A:2.67			Not in mitomap	Not in mtDB
13,933	ND5	A > G	A:0.3 > G:99.4	ACA > GCA	T533A	reported	mtDB, 2700:4
14,470	ND6	T > C	T:78.7 > C:21.2	GGA > GGG	G68G	reported	mtDB, 2628:68
15,218	CYTB	A > G	A:0.2 > G:99.6	ACA > GCA	T158A	reported	mtDB, 2665:38
15,326	CYTB	A > G	A:0.2 > G:99.6	ACA > GCA	T194A	reported	mtDB, 17:2687
16,067	HV1, d-loop	C > T	C:0.4 > T:99.6			reported	mtDB, 1864:3
16,362	HV1	T > C	T:0.1 > C:99.6			reported	mtDB, 1422:444

The novel mitochondrial variant, m.12302C > A (mt-tRNALeu(CUN)), which was detected at a low level of heteroplasmy (2.67%) in blood and in dermal fibroblasts (2.7%), is highlighted in yellow, while the rare homoplasmic variant, m.13933A > G, reported as a polymorphism in Mitomap is highlighted in grey.

Table 2
Results of Whole Exome Sequencing using proband's fibroblasts.

Gene	Disease	Variant	Nucleotide	Inheritance pattern	Zygosity	Reference	Classification
GALT	Galactosemia	p.Q188R	c.563 A > G	AR	Het (paternal)	rs75391579	Pathogenic
GALT	Galactosemia	N/A	c.-119_-116delGTCA	AR	Het (maternal)	rs111033640	Pathogenic
GALT	Galactosemia	p.N314D	c.940 A > G	AR	Het (maternal)	rs2070074	Pathogenic
RYR1	Malignant hyperthermia Susceptibility	p.G2434R	c.7300G > A	AD	Het (maternal)	rs121918593	Pathogenic
PNKD	Paroxysmal nonkinesigenic dyskenesia	p.L18F	c.52C > T	AD	Het (maternal)	Novel variant	VUS
MTO1	Combined oxidative phosphorylation deficiency	p.T207M	c.620C > T	AR	Het (Maternal)	rs139334277	VUS
NDUFA2	Leigh Syndrome/ Complex I deficiency	p.P63L	c.188C > T	AR	Het (paternal)	Novel variant	VUS

Abbreviation: AD: Autosomal dominant; AR: Autosomal recessive; Het: Heterozygous; VUS: Variant of Unknown Significance.

3.3. Functional studies of the ATP metabolism

In light of the analyses of the proband's nuclear and mitochondrial genomes by massively parallel sequencing along with the suspected AHC mitochondrial etiology, we investigated the proband's ATP metabolism using dermal fibroblasts. As a control subject, we used commercially available dermal fibroblasts from a healthy subject whose metabolic profile has already been characterized and comparable to two other healthy subjects [13] [Uittenbogaard et al., 2018]. We utilized the Seahorse Extracellular Flux XFp analyzer for live-cell measurement of OCR, a key functional indicator of the mitochondrial energy metabolism. We performed the real-time live-cell Mitochondrial Stress Test assay to accurately measure OXPHOS bioenergetic parameters (Fig. 4A, B). Even though the basal and ATP-linked respiration levels were normal in the proband's fibroblasts, we detected a significant deficit in two key bioenergetic parameters responsible to stimulate the OXPHOS metabolism upon energy demand to avert an ATP crisis (Fig. 4C). We quantified the maximal respiratory capacity elicited by the protonophore FCCP and found a 27% decrease when compared to that of the healthy subject. More notably, the proband's fibroblasts exhibited a 60% loss of spare respiratory capacity, which severely curtailed the proband's bioenergetic capacity to thwart an energy crisis (Fig. 4C). Collectively, our results indicate that the proband's fibroblasts only have the bioenergetic capacity to ensure basal ATP homeostasis,
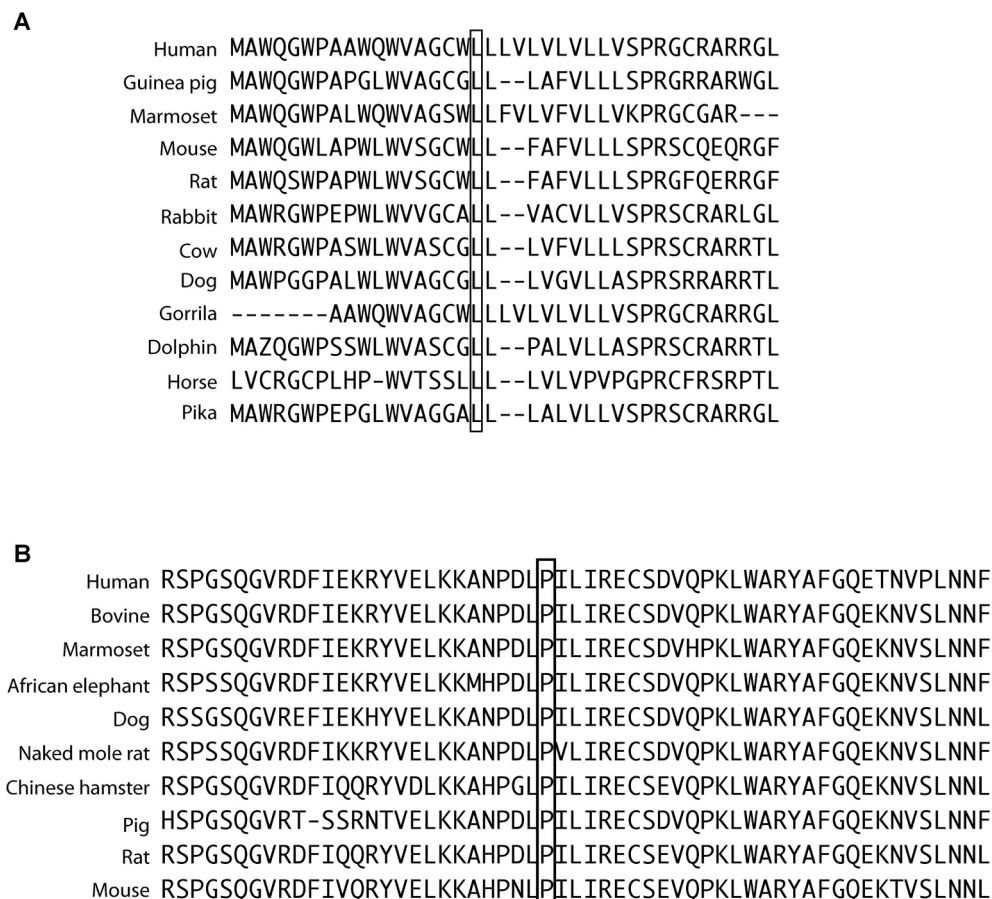

Fig. 3. Sequence alignment of mammalian homologs of the PKND (A) and NDUFA2 (B) proteins showing conservation of the mutated amino acids depicted with a bracket.
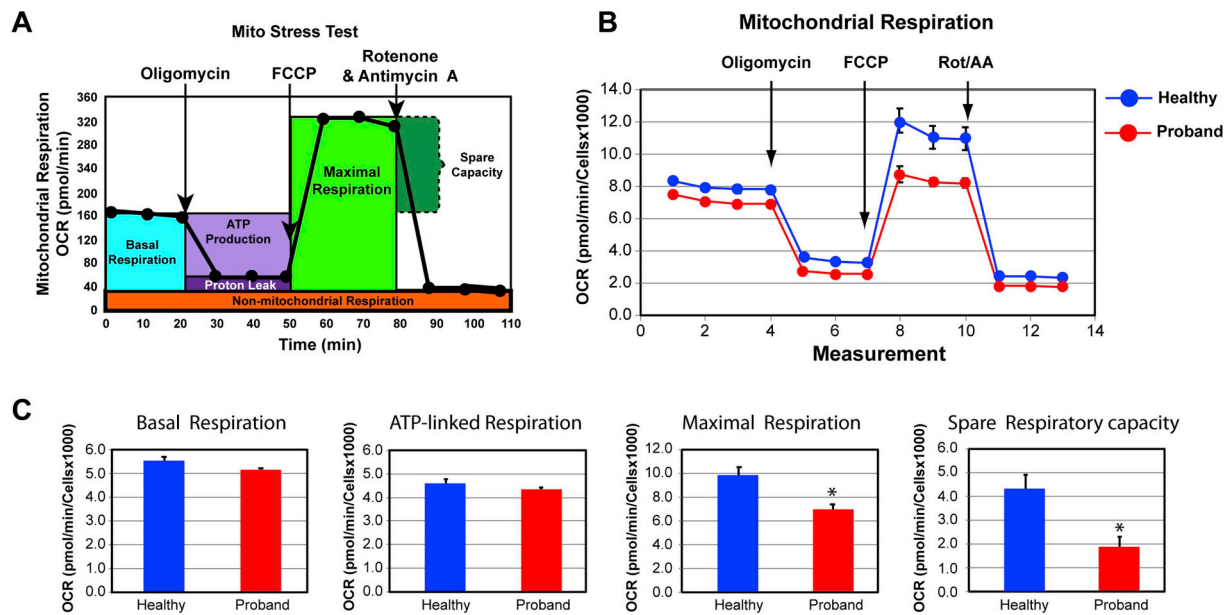
Fig. 4. The proband's fibroblasts exhibit an impaired bioenergetic capacity. A. Profile of the oxygen consumption rate (OCR) adapted from the Agilent Technologies brochure of the Mitochondrial Stress Test. B. OCR profiles of the proband (red) and healthy subject (blue). C. Quantitative data of basal respiration, ATP-linked respiration, maximal respiration, and spare respiratory capacity. The healthy subject is shown in blue while the the proband is illustrated in red. Data are represented as means ± S.E.M., n = 3 of independent experiments, each with three technical replicates. * indicates statistically significant differences with a p value of 0.0001.

which is insufficient to avoid an ATP crisis upon high energy expenditure as a result of the profound deficit in spare respiratory capacity.

We next examined the rate of ATP production in the proband's fibroblasts from the two major pathways glycolysis and OXPHOS. We took advantage of the Seahorse XFp Real-Time ATP rate assay, which allows concurrent quantification of rates of ATP production from these two pathways in live cells. Both OCR and ECAR were simultaneously measured upon injection of oligomycin, an inhibitor of the ATP synthase, followed by injection of rotenone and antimycin A to fully inhibit mitochondrial ATP production (Fig. 5A). As expected, the basal rate of ATP production from OXPHOS in the proband's fibroblasts was identical to that of a healthy subject's fibroblasts (Fig. 5B), confirming our results from the Mitochondrial Stress Test assay (Fig. 4). However, we

Fig. 5. The proband and a healthy subject display distinct energy metabolic phenotypes. A. Schematic representation of the Agilent Seahorse XFp Real-Time ATP rate assay. Both OCR and ECAR of live fibroblasts derived from the proband or a healthy subject are simultaneously measured upon compound injections of mitochondrial inhibitors, oligomycin followed by a mixture of rotenone and antimycin A. B. Quantification of ATP basal rate from glycolysis (blue for the healthy subject and red for the proband) and mitochondrial OXPHOS metabolism (blue hatched column for the healthy subject and red hatched column for the proband). Data are represented as means ± S.E.M., n = 3 of independent experiments, each with three technical replicates. * indicates statistically significant differences with a p value of 0.0001.

detected a 41% decrease in the basal rate of ATP production from glycolysis. Collectively, our results reveal a distinct energy phenotype of the proband's fibroblasts when compared to that of healthy fibroblasts.

We further investigated the glycolytic metabolism in the proband's fibroblasts using the Glycolysis Rate assay. It directly and accurately assesses glycolytic activity by correlating one-to-one with lactate accumulation. The total Proton Efflux Rate (PER) and the Glycolytic Proton Efflux Rate (GlycoPER) were measured using both OCR and ECAR values in order to account for mitochondrial (CO_2) acidification from the mitochondrial TCA cycle making up for some of the acidification of the medium (Fig. 6A, B) [19]. In the absence of mitochondrial OXPHOS inhibitors, the proband's fibroblasts exhibited a severe decrease in basal glycolysis by 52% when compared to that of healthy fibroblasts (Fig. 6C). This is further corroborated by the proband's fibroblasts having a lower %PER from basal glycolysis than the healthy fibroblasts (Fig. 6C). We next investigated whether the proband's fibroblasts could undergo metabolic reprogramming toward glycolysis following an energy crisis provoked by full inhibition of mitochondrial ATP production by rotenone and antimycin A. We found that the proband's fibroblasts exhibited a reduced compensatory glycolytic response by 34% when compared to that of healthy fibroblasts. Our collectively results reveal that the proband's fibroblasts could not switch to glycolysis upon an acute OXPHOS metabolic crisis to sustain ATP homeostasis.

3.4. Mitochondrial morphometric analysis of the proband's fibroblasts

In light of the dysregulated mitochondrial energy phenotype of the proband's fibroblasts, we investigated by transmission electron microscopy whether the proband's mitochondria exhibited ultrastructural defects. As expected, fibroblasts from the healthy subjects contain healthy long mitochondria with numerous cristae and an electron-dense mitochondrial matrix. The proband's fibroblast harbor mitochondria with normal and abnormal morphology (Fig. 7A). Healthy mitochondria are elongated with a normal ultrastructural morphology characterized by numerous cristae and a highly electron dense mitochondrial matrix (Fig. 7B). In contrast, the diseased mitochondria exhibited
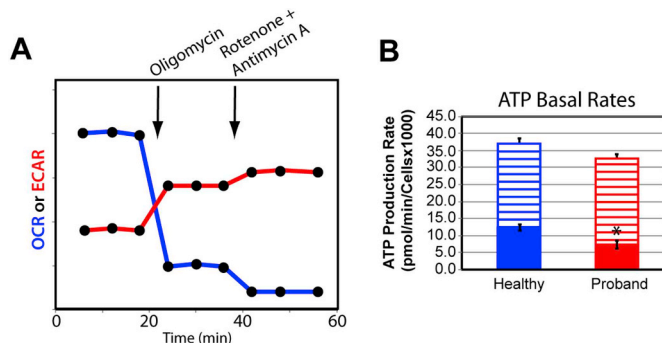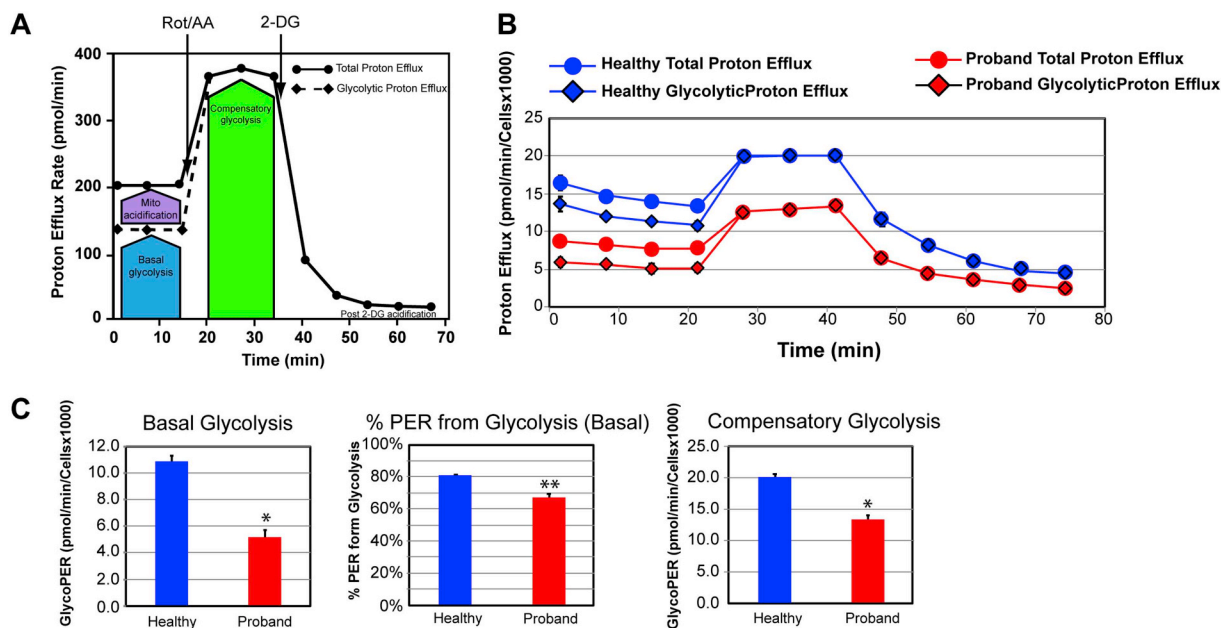
Fig. 6. The proband's fibroblasts exhibit altered proton efflux rate. A. Schematic representation of the Agilent Seahorse XFp Glycolytic Rate assay adapted from the Agilent Technologies brochure. B. Profiles of the proton efflux rate (PER) of the proband (red) and a healthy subject (blue). C. Quantitative analysis of three key bioenergetic markers for glycolysis: basal glycolysis, %PER from basal glycolysis, and compensatory glycolysis (healthy subject in blue and proband in red). Data are represented as means ± S.E.M., n = 3 of independent experiments, each with three technical replicates. * and **indicate statistically significant differences with a *p* value of 0.0001 or 0.0008, respectively.

rare and short cristae that appeared disorganized and a less electron dense matrix (Fig. 7C). In addition, the proband's fibroblasts have endoplasmic reticulum (ER) with enlarged saccules, indicative of ER stress (Fig. 7). Thus, our mitochondrial morphometric findings are congruent with our live-cell OCR measurements showing a decreased mitochondrial bioenergetic capacity (Fig. 4).

4. Discussion

Our study reports a patient clinically diagnosed with an atypical form of alternating hemiplegia of childhood (AHC) presenting symptoms suggestive of a mitochondrial etiology and of an unclear genotype-phenotype correlation given the absence of the *ATP1A3 ATP1A2* and
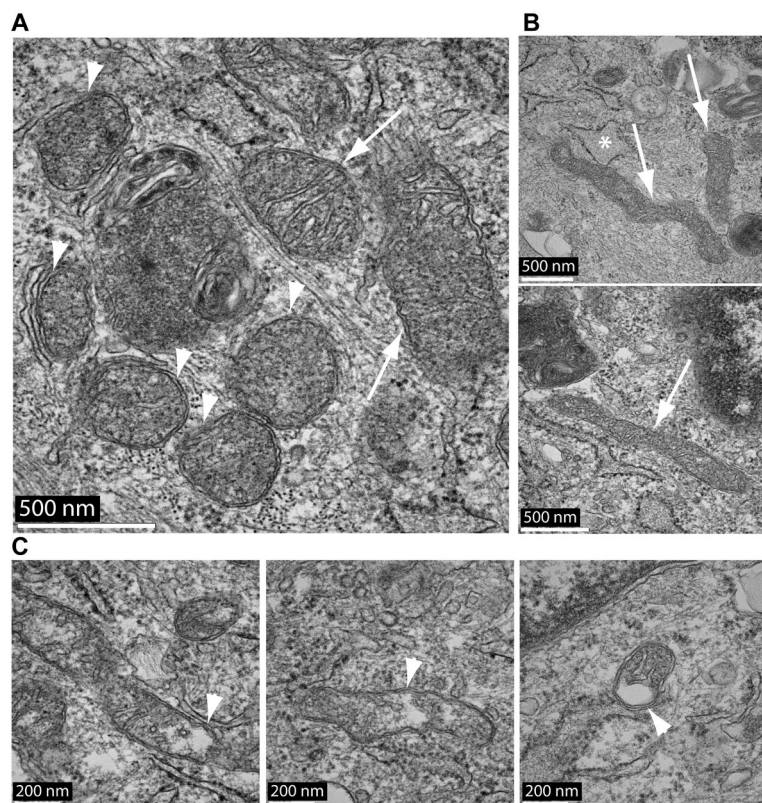

Fig. 7. Mitochondrial morphometric analysis of the proband's fibroblasts by transmission electron microscopy. A. The proband's fibroblasts harbor a mixed population of mitochondria with normal (white arrow) and abnormal (white arrowhead) cristae morphology. Scale bar = 500 nm. B. Mitochondria with a normal cristae morphology and density (white arrow). Enlarged saccule of the endoplamic reticulum is indicated by a white asterisk. Scale bar = 500 μm. C. High magnification of mitochondria harboring cristae of altered density and length (white arrowhead). Scale bar = 200 μm. The scale bar is indicated at the bottom left corner of each micrograph.

GLUT1 pathogenic variants, known to account for the majority of sporadic AHC cases [4–6,20,21]. Although the proband harbors three distinct pathogenic variants mapping in the *GALT* gene detected by WES, his galactosemia-related symptoms have no bearing on his clinical presentation of atypical AHC. Our WES analysis has yielded valuable genetic clues on the mitochondrial etiology of this atypical AHC by highlighting three variants detected in the *PNKD*, *MTO1* and *NDUFA2* nuclear genes, all involved in the mitochondrial energy metabolism. LR-PCR-NGS did not detect large structural rearrangements or deletions, nor any known pathogenic variants associated with a primary mitochondrial disease, such as MELAS (Mitochondrial Encephalopathy with Lactic Acidosis and Stroke-like episodes), thereby substantiating the normal brain MRI of the proband [22]. However, the proband's mitochondrial genome harbored a novel mitochondrial variant of unknown significance, m.12302C > A, which targets the *MT-TL2* gene encoding the mitochondrial tRNALeu(CUN), essential for mitochondrial protein translation. Unless the m.12302C > A variant is expressed at much higher levels of heteroplasmy in affected organs, such as muscles and brain, than in blood and dermal fibroblasts, it is unlikely to be the primary variant responsible for the overall mitochondrial etiology of AHC. However, we cannot exclude its potential secondary role in the AHC phenotypic manifestation when combined with the nuclear variants in the *PNKD*, *MTO1* and *NDUFA2* genes, all affecting the OXPHOS metabolism.

Although the pathogenic mechanisms of AHC have remained enigmatic, several studies have reported some mitochondrial dysfunctions in patients with AHC by MRS and muscle biopsy to measure enzymatic activities of the mitochondrial chain complexes, key players of the OXPHOS metabolism [11,12,23–25]. The original studies could not quantify this critical bioenergetic parameter in the absence of the Seahorse technology, which might have underestimated the number of patients with AHC with mitochondrial OXPHOS deficit. A recent WES-based study reports the presence of a homozygous *TANGO2* (transport and Golgi organization 2 homolog) pathogenic variant in a patient with AHC of unknown genetic diagnosis [26]. The TANGO2 protein being localized in mitochondria influences the mitochondrial energy metabolism [27,28].

Our live cell metabolic study provides the first evidence of a deficient energy metabolism due to a dysregulated interplay between glycolysis and OXPHOS, which may contribute to the progressive nature of the proband's AHC symptoms. The proband's fibroblasts exhibit a diminished metabolic plasticity preventing an efficient switch from OXPHOS to glycolysis to sustain ATP homeostasis under conditions mimicking an ATP crisis. The proband's fibroblasts display a diminished basal glycolysis, a deficit further exacerbated by a stunted compensatory glycolytic reserve response.

More notably, the proband's dermal fibroblasts display a dysregulated OXPHOS characterized by a major deficit in spare respiratory capacity, hindering their ability to avert an ATP crisis upon energy demand. This metabolic disturbance is keenly relevant to the fatigability, exercise intolerance, mental exhaustion and developmental regression exhibited by the proband (Fig. 1). Firing neurons utilize up to 80% of the spare respiratory capacity to prevent bioenergetic exhaustion [29]. Similarly, skeletal muscle cells are particularly susceptible to loss of the spare respiratory capacity, which leads to reduced physical activities and ultimately to sarcopenia [30]. The OXPHOS profile of the proband's fibroblasts is consistent with the mitochondrial morphometric analysis showing the presence of both normal and abnormal mitochondria in his fibroblasts. Mitochondria with a normal morphology display numerous cristae with a normal ultrastructure, while those with a perturbed morphology exhibit an altered cristae organization in terms of density and length. Since cristae house the OXPHOS machinery [31], abnormal crista ultrastructure has been correlated with dysfunctions in respiratory capacity [32].

The dysregulated OXPHOS signature of the proband's fibroblasts is also congruent with the WES results showing variants mapping in three genes relevant to OXPHOS metabolism. Of interest is the novel paternally inherited *PNKD* variant with an autosomal dominant mode of inheritance, which targets a highly conserved leucine residue mapping in the mitochondrial leading sequence of the encoded protein MR-1 [17]. Similarly to the proband's fibroblasts, fibroblasts from pediatric patients with paroxysmal nonkinesigneic dyskinesias (PNKD) caused by other *PKND* variants also exhibit a reduced maximal respiration and spare respiratory capacity without affecting the basal and ATP-linked respiration [17,33]. However, the fact that the proband's father is asymptomatic suggests that this novel *PNKD* variant cannot by itself induce OXPHOS dysregulation, leading to the AHC phenotypic expressivity in the proband. The father also harbors a novel heterozygous *NDUFA2* variant with an autosomal recessive inheritance pattern. By itself it cannot not alter OXPHOS activity, as only homozygous or compound heterozygous *NDUFA2* variants induce a severe complex I deficiency in patients with leukoencephalopathy or Leigh syndrome [18,34,35]. This is most likely due to the fact that NDUFA2 is an accessory subunit involved in the last step of complex I biogenesis to favor complex I stability rather than its activity [36–39].

Thus, our genetic analyses suggest three potential genetic etiologies to the AHC phenotypic expressivity in the proband is most likely caused by the combinatorial effects from nuclear variants inherited both from the father and mother, primarily detected in genes known to alter the mitochondrial energy metabolism. Since the asymptomatic mother solely harbors the heterozygous *MTO1*variant with an autosomal recessive transmission pattern, it is plausible that it acts as modifier of expressivity by exacerbating the metabolic phenotypic expression of the *PNKD* and *NDUFA2* variants. This *MTO*1 variant is detected in a gene encoding the mitochondrial tRNA translation optimization 1, known to cause combined oxidative phosphorylation deficiency 10 (COXPD10; OMIM 614702).

In summary, our metabolic and genetic studies suggest four possible genetic scenarios to modulate the phenotypic expressivity of this atypical AHC to be deciphered in our future studies: 1) synergistic heterozygosity among the three identified heterozygous nuclear variants and the mitochondrial variant m.12302C > A potentiating its low heteroplasmy; 2) synergistic heterozygosity due to all heterozygous variants affecting mitochondrial functions; 3) the heteroplasmic levels of the novel m.12302C > A variant of unknown clinical significance could be elevated in the affected tissues, such as brain and muscle; and 4) yet to be identified nuclear DNA defects that could be intronic or regulating RNA expression, which could be identified by whole genome sequencing. Thus, our studies provide novel insights into the pathophysiological mechanisms of AHC with a suspected mitochondrial etiology and undefined genotype-phenotype correlation. Our results also shed light on the impact of dysregulated metabolic reprograming on the progressive nature of the proband's mitochondrial phenotype, thereby providing clues to advance our understanding of the clinical phenotypic heterogeneity characteristic of AHC. This will lead to the recruitment of these patients in existing clinical studies targeted for mitochondrial diseases and ultimately to the design of novel therapeutic strategies.

Declaration of competing interest

The authors declare that they have no conflict of interest.

References

[1] S. Verret, J.C. Steele, Alternating hemiplegia in childhood: a report of eight patients with complicated migraine beginning in infancy, Pediatrics 47 (1971) 675–680.

[2] M. Bourgeois, J. Aicardi, F. Goutieres, Aletrnating hemiplegia of childhood, J. Pediatr. 122 (1993) 673–679.

[3] E.L. Heinzen, A. Arzimanoglou, A. Brashear, S.J. Clapcote, F. Gurrieri, D.B. Goldstein, S.H. Jóhannesson, M.A. Mikati, B. Neville, S. Nicole, L.J. Ozelius, H. Poulsen, T. Schyns, et al., Distinct neurological disorders with *ATP1A3* mutations, Lancet Neurol. 13 (2014) 503–514.

[4] E.L. Heinzen, K.J. Swoboda, Y. Hitomi, F. Gurrieri, S. Nicole, B. de Vries, F.D. Tiziano, B. Fontaine, N.M. Walley, S. Heavin, E. Panagiotakaki, et al., *De novo* mutations in ATP1A3 cause alternating hemiplegia of childhood, Nat. Genet. 44 (2012) 1030–1034.

[5] H. Rosewich, H. Thiele, A. Ohlenbusch, U. Maschke, J. Altmüller, P. Frommolt, B. Zirn, F. Ebinger, H. Siemes, P. Nürnberg, K. Brockmann, J. Gärtner, Heterozygous de novo mutations in ATP1A3 in patients with alternating hemiplegia of childhood: a whole exome sequencing gene-identification study, Lancet Neurol. 11 (2012) 764–773.

[6] A. Ishii, Y. Saito, J. Mitsui, H. Ishiura, J. Yoshimura, H. Arai, S. Yamashita, S. Kimura, H. Oguni, S. Morishita, S. Tsuji, M. Sasaki, S. Hirose, Identification of ATP1A3 mutations by exome sequencing as the cause of alternating hemiplegia of childhood in Japanese patients, PLoS ONE 8 (2013) e56120, , https://doi.org/10.1371/journal.pone.0056120.

[7] E. Kanavakis, A. Xaidara, D. Papathanasiou-Klontza, A. Papadimitriou, S. Velentza, S. Youroukos, Altenating hemiplegia of childhood: a syndrome inherited with an autosomal dominant trait, Dev. Med. Child Neurol. 45 (2003) 833–836.

[8] M.T. Bassi, N. Bresolin, A. Tonelli, K. Nazos, F. Crippa, C. Baschirotto, C. Zucca, A. Bersano, D. Dolcetta, F.M. Boneschi, V. Barone, G. Casari, A novel mutation in the *ATP1A2* gene causes alternating hemiplegia of childhood, J. Med. Genet. 41 (2004) 621–628.

[9] K.J. Swoboda, E. Kanavakis, A. Xaidara, J.E. Johnson, M.F. Leppert, M.B. Schlesinger-Massart, L.J. Ptacek, K. Silver, S. Youroukos, Alternating hemiplegia of childhood or familial hemiplegic migraine? A novel *ATP1A2* mutation, Ann. Neurol. 55 (2004) 884–887.

[10] G.J. Kemp, D.J. Taylor, P.R. Barnes, J. Wilson, G.K. Radda, Skeletal muscle mitochondrial dysfunction in alternating hemiplegia of childhood, Ann. Neurol. 38 (1995) 681–684.

[11] M.T. Sweney, K. Silver, M. Gerard-Blanluet, J.M. Pedespan, F. Renault, A. Arzimanoglou, M. Schlesinger-Massart, A.J. Lewelt, S.P. Reyna, K.J. Swoboda, Alternating hemiplegia of childhood: early characteristics and evolution of a neurodevelopmental syndrome Pediatrics, 123 (2009), p. e535, https://doi.org/10.1542/peds.2008-2027.

[12] C. Fons, J. Campistol, E. Panagiotakaki, M. Giannotta, A. Arzimanoglou, G. Gobbi, B. Neville, F. Ebinger, S. Nevšímalová, L. Laan, P. Casaer, G. Spiel, M. Ninan, G. Sanje, R. Artuch, T. Schyns, R. Vavassori, et al., Alternating hemiplegia of childhood: metabolic studies in the largest European series of patients, Eur. J. Paediatr. Neurol. 16 (2012) 10–14.

[13] M. Uittenbogaard, C.A. Brantner, Z. Fang, L.-J. Wong, A. Gropman, A. Chiaramello, Novel insights into the functional metabolic impact of an apparent *de novo* m.8993T>G variant in the *MT-ATP6* gene associated with maternally inherited form of Leigh syndrome, Mol. Genet. Metab. 124 (2018) 71–81.

[14] H. Cui, F. Li, D. Chen, G. Wang, C.K. Truong, G.M. Enns, B. Graham, M. Milone, M.L. Landsverk, J. Wang, W. Zhang, L.J. Wong, Comprehensive next-generation sequence analyses of the entire mitochondrial genome reveal new insights into the molecular diagnosis of mitochondrial disorders, Genet. Med. 5 (2013) 388–394.

[15] M. Uittenbogaard, H. Wang, V.W. Zhang, L.J. Wong, C.A. Brantner, A. Gropman, A. Chiaramello, The nuclear background influences the penetrance of the near-homoplasmic m.1630 a>G MELAS variant in a symptomatic proband and asymptomatic mother, Mol. Genet. Metab. 126 (2019) 429–438.

[16] J.R. Lopez, V. Kaura, C.P. Diggle, P.M. Hopkins, P.D. Allen, Malignat hyperthermia, environmental heat stress, and intracellular calcium dysregulation in a mouse model expressing the p.G2435R variant of RYR1, Br. J. Anaesth. 121 (2018) 953–961.

[17] D. Guezzi, C. Viscomi, A. Ferlini, F. Gualandi, P. Mereghetti, D. DeGrandis, M. Zeviani, Paroxysmal non-kinesigenic dyskinesia is caused by mutations of the MR-1 mitochondrial targeting sequence, Hum. Mol. Genet. 18 (2009) 1058–1064.

[18] A.J.G. Hoefs, C.E.J. Dieteren, F. Distlemaier, R.J. Janssen, A. Epplen, H.G.P. Swarts, M. Forkink, R.J. Rodenburg, L.G. Nijtmans, P.H. Willems, J.A.M. Smeitink, L.P. van den Heuvel, NDUFA2 complex I mutation leads to Leigh disease, Am. J. Hum. Genet. 82 (2008) 1306–1315.

[19] S.A. Mookerjee, A.A. Gerencser, D.G. Nicholls, M.D. Brand, Quantifying intracellular rates of glycolytic and oxidative ATP production and consumption using extracellular flux measurements, J. Biol. Chem. 292 (2017) 7189–7207.

[20] C.L. Bizec, S. Nicole, E. Panagiotakaki, N. Seta, S. Vuillaumier-Barrot, No mutation in the *SLC2A3* gene in cohorts of GLUT1 deficiency syndrome-like patients negative for SLC2A1 and in patients with AHC negative for ATP1A3, in: J. Zschoke, K. Gibson, G. Brown, E. Morava, V. Peters (Eds.), JIMD Reports, 12 2014, pp. 115–120 Springer, Cham.

[21] X. Yang, H. Gao, J. Zhang, X. Xu, X. Liu, X. Wu, L. Wei, Y. Zhang, ATP1A3 mutations and genotype-phenotype correlation of alternating hemiplegia of childhood in Chinese patients, PLoS ONE 9 (2014) e97274, , https://doi.org/10.1371/journal.pone.0097274.

[22] A.L. Gropman, Neuroimaging in mitochondrial disorders, Neurotherapeutics 10 (2013) 273–285.

[23] D.L. Arnold, K. Silver, F. Andermann, Evidence for mitochondrial dysfunction in patients with alternating hemiplegia of childhood, Ann. Neurol. 33 (1993) 604–607.

[24] M.A. Mikati, U. Kramer, M.L. Zupanc, R.J. Shanahan, Alternating hemiplegia of childhood: clinical manifestations and long-term outcome, Pediatr. Neurol. 23 (2000) 134–141.

[25] A. Bhatt, S. DeRoos, K. Chillag, Alternating hemiplegia of childhood with mitochondrial dysfunction: response to coenzyme Q10, Eur. Paediatr. Neurol. 11 (2007) 127–128.

[26] K. Sen, M. Hicks, A.H.M. Huq, R. Agarwal, Homozygous TANGO2 single nucleotide variants presenting with additional manifestations resembling alternating hemiplegia of childhood-expanding the phenotype of a recently reported condition, Neuropediatrics 50 (2019) 122–125.

[27] T.M. Maynard, D.W. Meechan, M.L. Dudevoir, D. Gopalakrishna, A.Z. Peters, C.C. Heindel, T.J. Sugimoto, Y. Wu, J.A. Lieberman, A.S. Lamantia, Mitochondrial localization and function of a subset of 22q11 deletion syndrome candidate genes, Mol. Cell. Neurosci. 39 (2008) 439–451.

[28] E. Jennions, C. Hedberg-Oldfors, A.K. Berglund, G. Kollberg, C.J. Törnhage, E.A. Eklund, A. Oldfors, P. Verloo, A.V. Vanlander, L. De Meirleir, S. Senecca, F.H. Sterky, N. Darin, TANGO2 deficiency as a cause of neurodevelopmental delay with indirect effects on mitochondrial energy metabolism, J. Inhert. Metab. Dis. 42 (2019) 898–908.

[29] D.G. Nicholls, Mitochondrial function and dysfunction in the cell: relevance to aging and aging-related disease, Int. J. Biochem. Cell Biol. 34 (2002) 1372–1381.

[30] A. Hiona, A. Sanz, G.C. Kujoth, R. Pamplona, A.Y. Seo, T. Hofer, S. Someya, T. Miyakawa, C. Nakayama, A.K. Samhan-Arias, S. Servais, J.L. Barger, M. Portero-Otin, M. Tanokura, T.A. Prolla, C. Leeuwenburgh, Mitochondrial DNA mutations induce mitochondrial dysfunction, apoptosis and sarcopenia in skeletal muscle of mitochondrial DNA mutator mice, PLoS ONE 5 (2010) e11468, , https://doi.org/10.1371/journal.pone.0011468.

[31] S. Cogliati, J.A. Enriquez, L. Scorrano, Mitochondrial cristae: where beauty meets functionality, Trends Biochem. 41 (2016) 261–273.

[32] J. Nielsen, K.D. Gejl, M. Hey-Mogensen, H.C. Holmberg, C. Suetta, P. Krustrup, C.P.H. Elemans, N. Ortenblad, Plasticity in mitochondrial cristae density allows metabolic capacity modulation in human skeletal muscle, J. Physiol. 595 (2017) 2839–2847.

[33] D. Guezzi, C. Canavese, G. Kovacevic, D. Zamurovic, C. Barzaghi, C. Giorgi, G. Zorzi, P. Zeviani, B. Garavaglia, N. Nardocci, A family with paroxysmal non-kinesigenic dyskinesias (PNKD): evidence of mitochondrial function, Eur. J. Paediatr. Neurol. 19 (2015) 64–68.

[34] A. Vanderver, C. Simons, G. Helman, J. Crawford, N.I. Wolf, G. Bernard, A. Pizzino, J.L. Schmidt, A. Takanohashi, D. Miller, A. Khozam, V. Rajan, et al., Whole exome sequencing in patients with white matter abnormalities, Ann. Neurol. 79 (2016) 1031–1037.

[35] S. Perrier, L. Gauquelin, M. Tétreault, L.T. Tran, N. Webb, M. Srour, J.J. Mitchell, C. Brunel-Guitton, J. Majewski, V. Long, S. Keller, M.J. Gambello, C. Simons, Care4 Canada Consortium, A. Vanderver, Recessive mutations in NDUFA1 cause mitochondrial leukoencephalopathy, Clin. Genet. 93 (2018) 390–400.

[36] C.E.J. Dieteren, W.J.H. Koopman, H.G. Swarts, J.G.P. Peters, P. Maczuga, J.J. van Gemst, R. Masereeuw, J.A.M. Smeitink, L.G.J. Nijtmans, P.H.G.M. Willems, Subunit-specific incorporation efficiency and kinetics in mitochondrial complex I homeostasis, J. Biol. Chem. 287 (2012) 41852–41860.

[37] M. Mimaki, X. Wang, M. McKenzie, D.R. Thorburn, M.T. Ryan, Understanding mitochondrial complex I assembly in health and disease, Biochim. Byophys. Acta 1817 (2012) 851–862.

[38] B. Andrews, J. Carroll, S. Ding, I.M. Fearnley, J.E. Walker, Assembly factors for the membrane arm of human complex I, Proc. Natl. Acad. Sci. USA110 (2013) 18934–18939.

[39] S. Guerrero-Castillo, F. Baertling, D. Kownatzki, H.J. Wessels, S. Arnold, The assembly pathway of mitochondrial respiratory chain complex I, Cell Metab. 25 (2017) 128–139.